coatings

MDPI

Article

Design and Analysis of a 5-Degree of Freedom (DOF) Hybrid Three-Nozzle 3D Printer for Wood Fiber Gel Material

Jifei Chen [1,*,†], Qiansun Zhao [1,†], Guifeng Wu [1], Xiaotian Su [1], Wengang Chen [1] and Guanben Du [2,*]

[1] School of Mechanical and Transportation, Southwest Forestry University, Kunming 650224, China; zhaoqiansun@swfu.edu.cn (Q.Z.); wuguifeng@swfu.edu.cn (G.W.); suxiaotian@swfu.edu.cn (X.S.); chenwengang999@swfu.edu.cn (W.C.)
[2] School of Material Science and Engineering, Southwest Forestry University, Kunming 650224, China
* Correspondence: cjf100cjf@swfu.edu.cn (J.C.); gongben9@hotmail.com (G.D.)
† These authors contributed equally to this work.

Abstract: Wood is an organic renewable natural resource. Cellulose, hemicellulose and lignin in wood are used in tissue engineering, biomedicine and other fields because of their good properties. This paper reported that the possibility of wood fiber gel material molding and the preparing of gel material were researched based on the wood fiber gel material as a 3D printing material. A five-degree of freedom hybrid three nozzle 3D printer was designed. The structural analysis, static analysis, modal analysis and transient dynamic analysis of 3D printers were researched, and the theoretical basis of the 3D printer was confirmed as correct and structurally sound. The results showed that the 5-DOF hybrid 3-nozzle 3D printer achieved the 3D printing of wood fiber gel material and that the printer is capable of multi-material printing and multi-degree-of-freedom printing.

Keywords: gel material; wood material; 3D printer; design and analysis

check for updates

Citation: Chen, J.; Zhao, Q.; Wu, G.; Su, X.; Chen, W.; Du, G. Design and Analysis of a 5-Degree of Freedom (DOF) Hybrid Three-Nozzle 3D Printer for Wood Fiber Gel Material. *Coatings* **2022**, *12*, 1061. https://doi.org/10.3390/coatings12081061

Academic Editor: Philippe Evon

Received: 6 June 2022
Accepted: 18 July 2022
Published: 27 July 2022

Publisher's Note: MDPI stays neutral with regard to jurisdictional claims in published maps and institutional affiliations.

Copyright: © 2022 by the authors. Licensee MDPI, Basel, Switzerland. This article is an open access article distributed under the terms and conditions of the Creative Commons Attribution (CC BY) license (https://creativecommons.org/licenses/by/4.0/).

1. Introduction

3D printing is an additive manufacturing technology used in aerospace, biomedicine, food, construction, industrial manufacturing, new materials and other fields [1]. As one of the technologies of the third industrial revolution, it has started to enter the consumer market after continuous development and research from the beginning of its development to the present day [2]. These 3D printers also have different structures and functions according to different materials. Currently, there are three main types of 3D printing materials, non-metallic materials, metallic materials and biomaterials. Among them, non-metallic materials mainly include photosensitive resins, polylactic acid, plastics, ceramics and so on. In pursuit of a green, low-carbon and sustainable development concept, researchers are also looking for natural materials for 3D printing. Wood, as a natural renewable resource, has attracted the attention of researchers. Through the rational use of tree resources, it can solve the material problem and add a way of wood utilization, which has important significance and good development prospects [3].

Wood is composed of primarily organic matter and a small amount of inorganic matter. The former includes mainly cellulose, hemicellulose and lignin, which may amount to over 90% of its biomass [4]. Cellulose, one of the main components of plants, is also the most naturally abundant and sustainable polymeric raw material. Due to its various excellent properties and wide range of sources, cellulose is already used in the commercial production of products. In the field of 3D printing, cellulose is also present in solid printing as a structural reinforcement [5], binder [6,7] and thickener [8].

Hemicellulose is a naturally occurring polysaccharide polymer, second only to cellulose, which is a branched amorphous heteropolysaccharide, consisting of five main types of xylan, glucomannan, arabinoglycan, galactan and dextran [9]. Despite being one of the most abundant natural polymers, hemicellulose is underutilised. Although hemicellulose

has great potential in the field of 3D printed condensation, there is currently very little 3D printing of hemicellulose. The main hemicellulose materials used for 3D printing are in their derivative form with other polymers for 3D printing [10] and require extensive chemical modification and various post-printing processes [11].

Like cellulose and hemicellulose, lignin is a natural polymer with reproducibility, biodegradability and biocompatibility. Lignin, a major component of chemical pulp black liquor, is the world's second most abundant natural polymer and the only renewable raw resource that contains considerable amounts of aromatic hydrocarbons [12]. The structural properties of lignin facilitate the synthesis of useful chemicals, fuels and low mass molecules and are also consistent with sustainable development and a reduced carbon footprint. It is attracting increasing global attention and is showing great economic potential for a variety of high-value bioproducts, including the 3D printing of biomaterials [13]. In terms of current research on the use of lignin and its derivatives as biomass materials for 3D printing, lignin can be physically or chemically blended with other components, such as polylactic acid (PLA) [14], to take advantage of the strengths of each material component after material compounding to achieve excellent 3D printing. Through chemical cross-linking, physical cross-linking and interpenetrating polymer network methods, wood gel materials are prepared for direct ink 3D printing and the complete printing of wood fiber gel materials. This is a new means of utilizing wood resources, which not only extends the range of 3D printing materials but also provides a new way to diversify the use of wood [15].

Due to the different properties of wood fiber gel materials, the forming mechanism of 3D printing and the structure and function of 3D printers are also different. In this study, wood fiber extracted from a branch, waste wood and wood scraps of Cunninghamia lanceolate. Using wood fiber gel material as the base material for 3D printing, the basic characteristics of wood fiber gel material printing and forming are studied, and a 3D printer corresponding to wood fiber gel material is designed according to the material characteristics, providing a way to use the wood resources. The 3D printer also has the ability to print three materials on the same platform with different printheads and is complemented by five degrees of freedom of movement for print versatility. Finally, it also provides equipment support for the subsequent wood fiber composite printing of biomimetic wood.

2. Materials and Methods

2.1. Materials and Equipment

Cellulose, hemicellulose and lignin were extracted from cedar wood powder. Sodium hydroxide (AR analytical purity-flakes, purity $\geq$ 96.0%), Chengdu Jinshan Chemical Reagent Co. Chitosan (AR analytical purity—off-white powder or flakes, purity $\geq$ 96.0%), Sinopharm Chemical Co. Acetic acid (AR analytical purity, purity $\geq$ 99.5%), Shanghai Aladdin Biochemical Technology Co. Urea (AR analytical purity—pellets, purity $\geq$ 99.0%), Sinopharm Chemical Co. Epichlorohydrin (AR Analytical purity, purity $\geq$ 98.0%), Shanghai Aladdin Biochemical Technology Co. Hydrochloric acid (AR analytical purity—liquid, purity $\geq$ 36.0%~38.0%), Shan Dian Pharmaceutical Co. Colouring agent (green), Guangdong Timothy Colour Food Colour Technology Co. Distilled water, homemade.

Collective thermostatic heating magnetic stirrer, Type DF-101S, Henan Province Yuhua Instruments Co. Rheometer: MARS III type, Germany HAAKE company. Vacuum drying oven: type DZF, Beijing Kewei Yongxing Instruments Co.

2.2. Cellulose Gel Material Preparation

An aqueous base system of sodium hydroxide, urea and distilled water (7:12:81 by mass) was used as the solvent, to which cellulose was added while stirring with an electromagnetic centrifugal stirrer until all the cellulose powder was dispersed in the solution and a milky-white solution without visible powder aggregates was formed. The

prepared cellulose suspension was stored in a refrigerator at −10 °C for 4–6 h and removed to obtain a clear cellulose gel [16,17] as shown in Figure 1a.

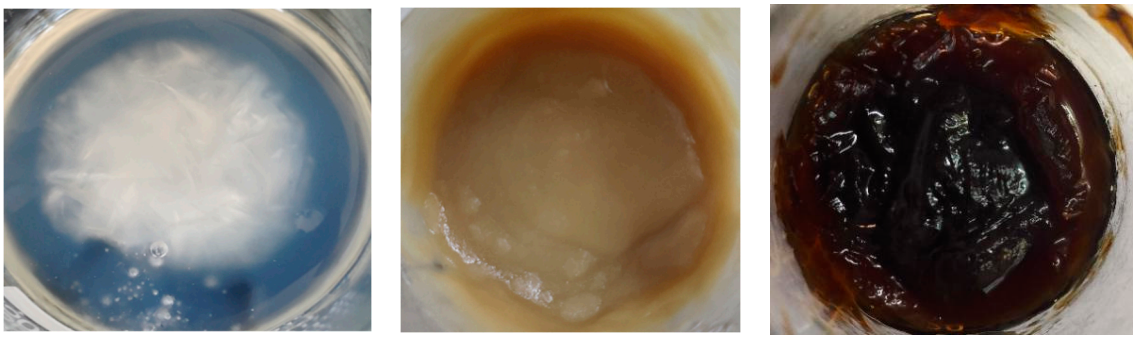

(**a**) (**b**) (**c**)

Figure 1. Wood fiber gel material. (**a**) Cellulose gel; (**b**) Hemicellulose gel; (**c**) Lignin gel.

2.3. Hemicellulose Gel Material Preparation

Mix hemicellulose and chitosan in a ratio of 6:4 in deionized water and add hydrochloric acid to adjust the pH value to 4. Heat the solution to 95 °C and keep it for 20 min to form a suspension of hemicellulose powder dissolved without cellulose suspension, then put it in the refrigerator at −12 °C for 4–6 h and take it out to prepare hemicellulose gel [18,19] as shown in Figure 1b.

2.4. Lignin Gel Material Preparation

Chitosan solution was prepared by dissolving 2.5 g of chitosan in 100 mL of 2.5 *v/v* % acetic acid, and lignin solution was prepared by dissolving 1 g of alkaline lignin in 10 mL of water. The chitosan solution and lignin solution were then mixed and chilled in a refrigerator at −10 °C for 5 h, and then removed and stored at 20 °C for half an hour to form a lignin gel [20] as shown in Figure 1c.

2.5. Rheology Tests

Using a HAAKE MARS III rheometer at a constant shear rate, cellulose gels (using a temperature ramp of 2 °C/min with a start temperature of 10 °C and measurements stopped at 80 °C) and hemicellulose gels (using a temperature ramp of 5 °C/min with a start temperature of 20 °C and measurements stopped at 140 °C), the pattern of viscosity change and maximum gelling temperature were measured. The gelling point was determined using Thermo Scientific HAAKE RheoWin software. (version 4.63.0004, Germany HAAKE company).

3. Results and Discussion

3.1. Gelation Point Analysis

The structural design of 3D printers is closely related to the forming materials, and the forming and curing mechanisms of different materials vary. For the analysis of wood gel material properties, the rheological properties of the material were experimented with the data obtained from the experiments and analyzed to obtain the characteristics of the wood fiber gel material, as shown in Figure 2.

Both cellulose and hemicellulose gels show a reduction in viscosity at the beginning of the test, which is a shear thinning characteristic and fits well with the printing characteristics of direct ink technology. This is a shear thinning characteristic that is very much in line with the printing characteristics of direct ink writing technology. It can also be seen that the wood fiber gel material shows a tendency to increase in viscosity with higher temperatures, and the graph shows that cellulose produced a mutation condition near 52 °C and hemicellulose produced a mutation near 80 °C. The reason for the mutation is due to the curing and

molding of the wood fiber gel material [21,22]. Therefore, in the process of designing 3D printers of wood fiber gel materials, the molding process needs to be designed around the material properties.

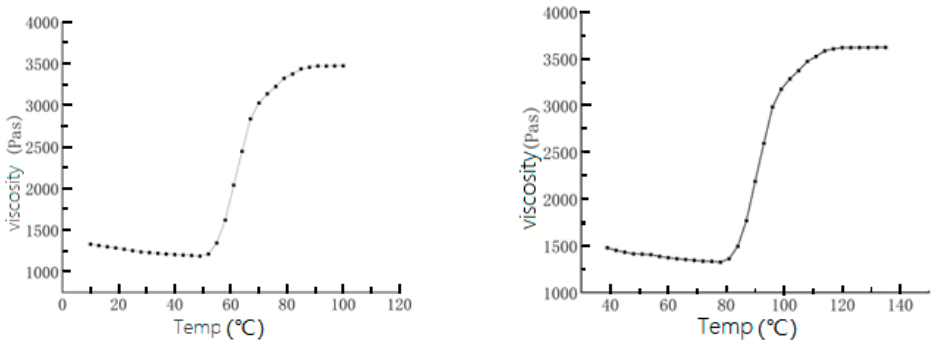

(**a**) (**b**)

Figure 2. Properties of wood fiber gel material. (**a**) Cellulose gel; (**b**) Hemicellulose gel.

3.2. Printer Type Selection

Currently, the main technologies applicable to the additive manufacturing of wood materials are FDM technology, which is used for hot-melt cold-set wood–plastic composites [22], and DIW technology, which is used for direct forming or externally formed flowing materials [23]. As the wood component prepared the printing material like a gel while combining different printing consumables, the researchers explored the use of external effects to assist the 3D printing process, such as light [23], rotation [24]. In addition, it can enable the 3D printing of materials, such as cyclopentadiene titanium [23] and short carbon fiber epoxy composites [24]. Those can further increase the additive technology applicability [25]. In Figure 3, 3D printer-assisted devices are shown. Based on the experimental data in Figure 2, it is also known that the prepared wood fiber gel materials have shear thinning properties. It is suitable for the DIW mode of printing. At the same time, based on the advantages of the DIW type of printing technology, assisted by the external action and the characteristics of the printing materials that we have studied, this type of wood fiber gel material can be extruded using an external laser to accelerate the curing of the wood fiber gel material. In addition, according to the study, the design of 3D printers should be biased towards the DIW type. For the design of 3D printers, multiple printheads are required to meet the design goals for cellulose gel materials, hemicellulose gel materials and lignin gel materials printed on the same model and on the same platform. The more common five-degree-of-freedom configuration was chosen to meet the development needs of 3D printers with multiple degrees of freedom.

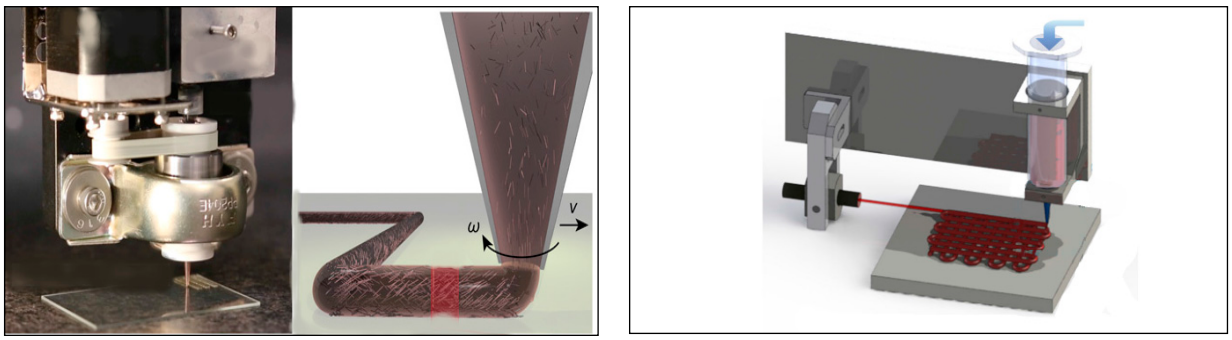

(**a**) (**b**)

Figure 3. 3D printer auxiliary equipment. (**a**) Rotating auxiliary devices [24]; (**b**) Laser auxiliary devices [23].

4. Structural Design and Description

4.1. Overall Structure

A 5-Degree of Freedom (DOF) hybrid three-nozzle 3D printer was designed based on the performance feature of wood fiber gel material. Its structure mainly includes a printing nozzle mechanism, a nozzle moving mechanism, a *z*-axis moving mechanism, a printing platform and a support frame. Wood fiber gel material was printed with three nozzles. The 3D printers that have multiple degrees of freedom and multiple nozzles have attracted increasing attention to meet the printing needs of a variety of materials [26,27]. Multi-nozzle 3D printers should be designed in such a way to ensure a smooth nozzle switch, smooth and accurate plane movement, accurate positioning of the nozzle, accurate platform control, etc. The structure of the 5-DOF hybrid three-nozzle 3D printer is illustrated in Figure 4.

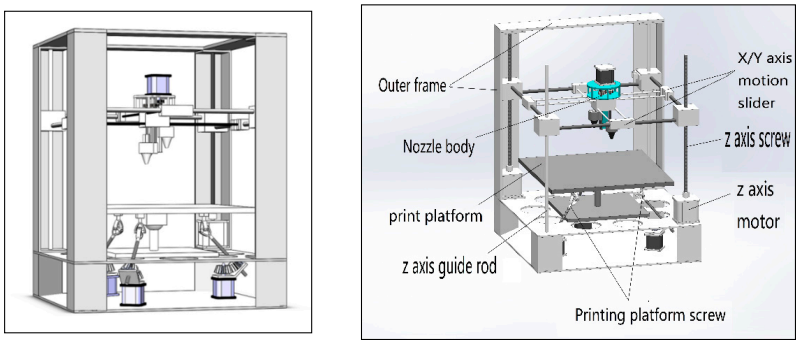

Figure 4. The 5-DOF hybrid three-nozzle 3D printer.

The movement of 3D printer nozzles mainly relies on the cross axis to realize the x and *y* axis movement in the plane, and the rotation of the screw rod is controlled by the stepper motor to drive the *z*-axis movement. Three nozzles are designed in the nozzle mechanism, which squeezes cellulose gel, Hemicellulose gel and lignin gel accurately, according to the computer structure diagram of the molding structure to a certain range; it can be a reduced material forming support structure by controlling the printer platform to move between $+45^{\circ}$ and -45°. The outer frame is the base that supports all mechanisms.

4.2. Design of Nozzle Mechanism

The nozzle mechanism is a core mechanism for the 3D printing of wood fiber gel material. Nozzle head mechanism includes nozzle head bracket, printer nozzle head, nozzle head switching motor and nozzle head switching gear group (Figure 5).

In the mechanism, the screw is driven by the motor and gear to move the three printer nozzles independently to make the print. The gear group of nozzle head switching is installed on the gearbox. The gear and shaft in the nozzle head switching gear group are made of non-magnetic materials. The output shaft of the nozzle switching motor is connected with the driving gear shaft through the telescopic shaft and matched with the spline. The electromagnet device comprises an electromagnet arranged on a driving gear and a magnet arranged in a gearbox. When the driving gear rotates, it drives the first gear to rotate and the second gear to rotate reversely, simultaneously, and then the screw connected to the two printer nozzles will rotate at the same time, but in the opposite direction. In addition, the two printer nozzles can move up and down in opposite directions. When the third print nozzle is needed, the first gear will rotate and the second switchgear will control the printer nozzle position to adjust to the central position. The electromagnet switch gear locates its axial position to make sure that the driving gear and the third switchgear will mesh, and starting the nozzle switch motor will engage the third printer head. By controlling the switch motor and electromagnetic mechanism of the nozzle, the three printer heads can be switched freely and can improve the printing efficiency and avoid the interference between the nozzles and the fixing frame while allowing the rapid switching of the three nozzles.

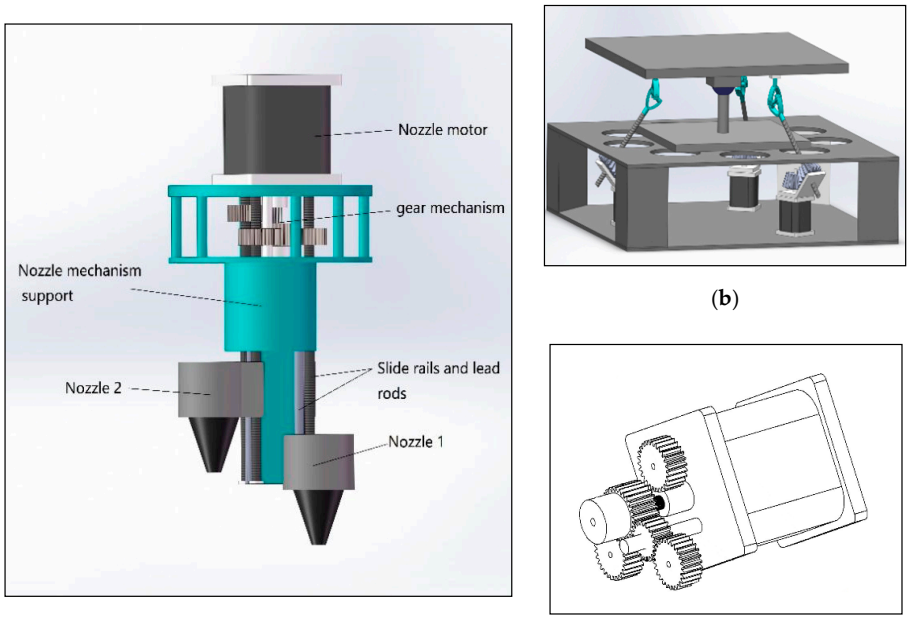

Figure 5. Printer nozzle mechanism. (**a**) Nozzle body; (**b**) Nozzle structure gear layout; (**c**) Printer platform mechanism.

4.3. Design of Printer Platform Mechanism

The printer platform mechanism makes the printing plate flip and tilt through a three-branch parallel mechanism and has two degrees of freedom of rotation in the *x* and *y* axis. It uses three stepping motors to drive the matching bevel gears, and then the bevel gear controls the platform screw to move, push and pull, and to drive the printer platform, so that the printing plate will complete the flip tilt. The parallel mechanism has three branches that are evenly distributed at 120° angle. Each branch of the parallel mechanism is driven by an independent motor that drives the screw to the required deflection of the printed platform. The printer platform mechanism can reduce the center of gravity of the 3D printer and can minimize the impact of vibration on the printing accuracy during motor operation, reduce the lateral force of the screw nut mechanism and effectively avoid screw deformation due to long-term stress, so that the printing accuracy is not affected (Figure 6).

The 3D printer is capable of increasing printing efficiency, reducing structural support and making prints of various types of materials.

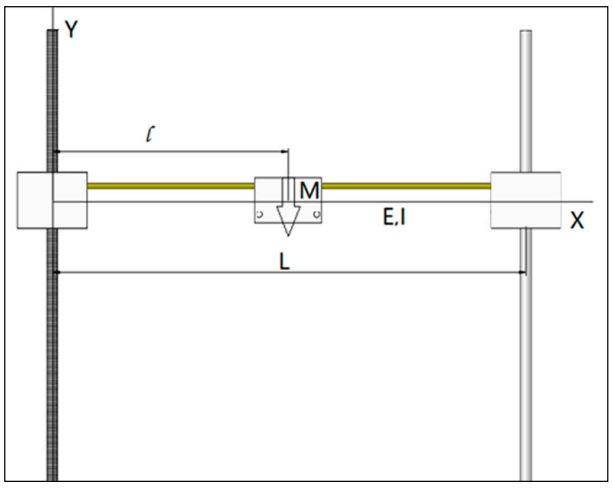

Figure 6. Schematic diagram of the simplified structure.

5. Structural and Mechanical Analysis

5.1. Degree of Freedom Analysis

The 3D printer is composed of the printing nozzle of a series of mechanisms and the printing platform of a parallel structure to form a 5-DoF motion. There are virtual constraints and local DoFs in its structure, and the modified CGK general DoF formula is used.

$$F = \mathrm{d}(n - g - 1) + \sum_{i=1}^{g} f_i + \mu - \zeta \tag{1}$$

where F is the degree of freedom of the mechanism; d is the order of mechanism (space mechanism d = 6); n is the number of components including the frame (the base included); g is the number of motion pairs; f_i is the degree of freedom of the i-th motion pair; μ is the virtual constraint number of mechanism; ζ is the local degree of freedom.

The parameters of the 3D printer were put into the Formula (1), and the freedom degree of the motion mechanism of the 5-DOF hybrid three-nozzle 3D printer was calculated to be five. The five DoFs are the xy plane DoF of the nozzle part and the cross axis structure, the vertical DoF of z-axis direction (3T), and the x and y axis rotation movement DoF of the derivative structure of Delta parallel structure of the printer platform part (2R), respectively. The 5-DoF hybrid three-nozzle 3D printer has 5 DoFs (3T-2R).

5.2. Statics Analysis

The equation of the deflection curve [28] is obtained based on the structural form of simply supported beams, and the maximum deflection is determined. The structure is simplified as a mass–spring system, and the cross-arm slides are simplified as a uniform cross beam (Figure 6).

The differential equation of the flexural function equation is established according to the structural reaction force (Formulas (2)–(4)). The quadratic integration is carried out, and the value of the constant term is obtained according to the boundary conditions, and the maximum deflection is finally obtained, as follows.

$$\left.\begin{aligned} EIw_1''(x) &= -\tfrac{F(L-l)}{L} \\ EIw_2''(x) &= -\tfrac{F(L-l)}{L}x + F(x-l)x \end{aligned}\right\} \tag{2}$$

$$\left.\begin{aligned} EIw_1'(x) &= -\tfrac{F(L-l)}{2L}x^2 + C_1 \\ EIw_2'(x) &= -\tfrac{F(L-l)}{2L}x^2 + \tfrac{1}{2}F(x-l)^2 + C_2 \end{aligned}\right\} \tag{3}$$

$$\left.\begin{aligned} EIw_1(x) &= -\tfrac{F(L-l)}{2L}x^3 + C_1x + D_1 \\ EIw_2(x) &= -\tfrac{F(L-l)}{2L}x^3 + \tfrac{1}{6}F(x-l)^3 + C_2x + D_2 \end{aligned}\right\} \tag{4}$$

where E is the elastic coefficient of the material, I is the moment of inertia of the section, L is the length of the transverse guide rod, l is the position of the nozzle at the guide rod, F is the force the rod received, w_i'' and w_i' are the second and first-order derivatives of the deflection, respectively.

The further calculation is made according to boundary conditions and continuous conditions. Because both ends of the guide rod are supported, the boundary conditions mainly consider both ends of the guide rod and its central position. Under continuous conditions, the left and right ends of the second and first order deflection differential equations are equal, respectively, in the central position, and the value of the constant is obtained.

Boundary condition,

$$l = 0;\ w = 0;\ l = \frac{1}{2}L;\ w_1 = w_2;\ l = L;\ w = 0;$$

Condition of continuity,

$$EIw_1'(l) = EIw_2'(l);\ C_1 = C_2 = \frac{F(L-l)}{6L}(2Ll - l^2);$$
$$EIw_1(l) = EIw_2(l);\ D_1 = D_2 = 0$$

$$\left.\begin{aligned} EIw_1(x) &= -\frac{F(L-l)}{2L}x^3 + \frac{F(L-l)}{6L}(2Ll - l^2)x \\ EIw_2(x) &= -\frac{F(L-l)}{2L}x^3 + \frac{1}{6}F(x-l)^3 + \frac{F(L-l)}{6L}(2Ll - l^2)x \end{aligned}\right\} \quad (5)$$

Given the proportional relationship between l and L, the maximum deflection can be obtained. When $l = \frac{1}{2}L$, $W_{\max} = \frac{FL^3}{48EI}$; When $l > \frac{1}{2}L$, $W_{\max} = \frac{F(L-l)}{9EIL}\sqrt{\frac{2Ll-l^2}{3}}$.

5.3. Modal Analysis

ANSYS software modal analysis function is used to analyze the dynamic characteristics of the 3D printer system. The structure dynamic characteristics of the 3D printer were analyzed and evaluated to ensure printing accuracy. The use of different materials for different parts of the structure will further affect the rationality of the 3D printer. The 3D printer's support and printing platform uses a 6063 aluminum alloy, while 45 steel is used for the guide, slider and screw. The 3D model of the 3D printer was constructed in Solid Works, and the structural model was imported into ANSYS analysis software to divide the mesh and optimize the mesh quality. The average quality index of grid elements is greater than 0.80, and the average aspect ratio is 1.93, which meets the requirements of structural field analysis (Figure 7).

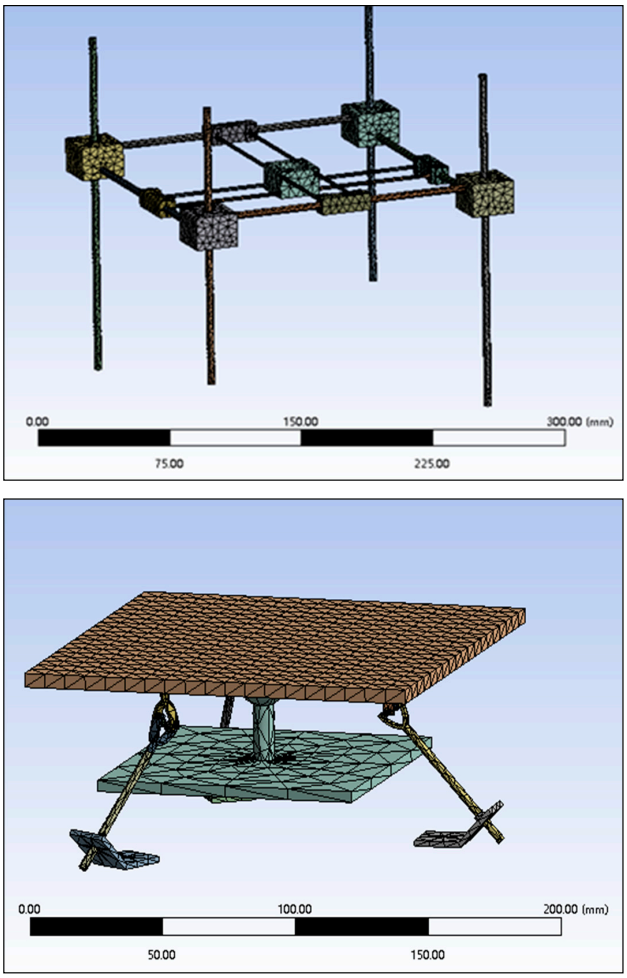

Figure 7. Meshing of kinematic mechanism of the ANSYS model.

The modal analysis of 3D printers is relatively fixed. The order of modal analysis is determined according to the modal calculation quality of each DoF and needs to be optimized and adjusted multiple times. The first eight order modal frequencies and the deformations of the 3D printer's motion mechanism are shown in Table 1.

Table 1. Modal frequency and deformation of the moving mechanism.

Order	Frequency/Hz	Deformation Behavior of XYZ Kinematic Mechanism Model	Order	Frequency/Hz	Printer Platform Mechanism Model Deformation
1	56.891	Pillar bent and deformed	1	74.119	Parallel branches move longitudinally
2	58.225	Pillar bent and deformed	2	74.317	Parallel branches move longitudinally
3	71.416	Guide rod deformed	3	74.327	Parallel branches move longitudinally
4	71.437	The guide rod deformed	4	74.602	Parallel branches move laterally
5	79.567	Overall torsion deformation occurred in the structure	5	74.982	Parallel branches move laterally
6	90.275	Guide rod deformed	6	75.162	Parallel branches move laterally
7	90.328	Guide rod deformed	7	103.57	Printer platform rotates along the *z*-axis
8	105.42	Guide rod deformed	8	133.76	Printer platform swings longitudinally

The results show that the deformation and natural frequency of models with different orders are different, which provides theoretical data support for subsequent design and manufacturing.

6. Transient Dynamics Analysis

3D printing is to drive each part to move by the motor, so as to drive the nozzle to move. In combination with the nozzle material extrusion and laser curing, the model printing molding is completed. In planning the printing paths and model slice processing, the reciprocating motion of the nozzle is inevitable, and the vibration generated therefrom will affect the printing accuracy. ANSYS Workbench software was used for the transient dynamics analysis of 3D printers, and structural deficiencies were improved to ensure structural stability and printing accuracy.

For nozzle movement, the influences of the *x*-axis and *y*-axis alone and the linkage of the two axes on the structure were analyzed. For *z*-axis, only the influence of its independent motion on the structure was analyzed. According to the motion characteristics, the total load step number was set to three in the software. The end times of the 1st, 2nd and 3rd load steps were 0.25 s, 0.75 s, and 1 s, respectively. The load was applied to the *z*-axis and analyzed in linkage with the *x* and *y* axis with added load. Since the motion of the *x*, *y* and *z* axes and the printing platform were independent, the single chain and multi-chain motion of the printer platform were simulated and the results analyzed.

(1) When *z*-axis moved, other motion axes were static or do not interfere with *z*-axis motion, and transient motion simulation was carried out when the *z*-axis moved independently. The results showed that the maximum displacement in the *z*-axis direction was close to the average displacement, and the motion accuracy in the *z*-axis direction was sufficient (Figure 8a). The movement displacement in the *x* and *y* axis directions was far less than the nozzle diameter, which secured accurate movement (Figure 8b,c). The motion displacement curve of the *z*-axis mechanism is shown in Figure 8.

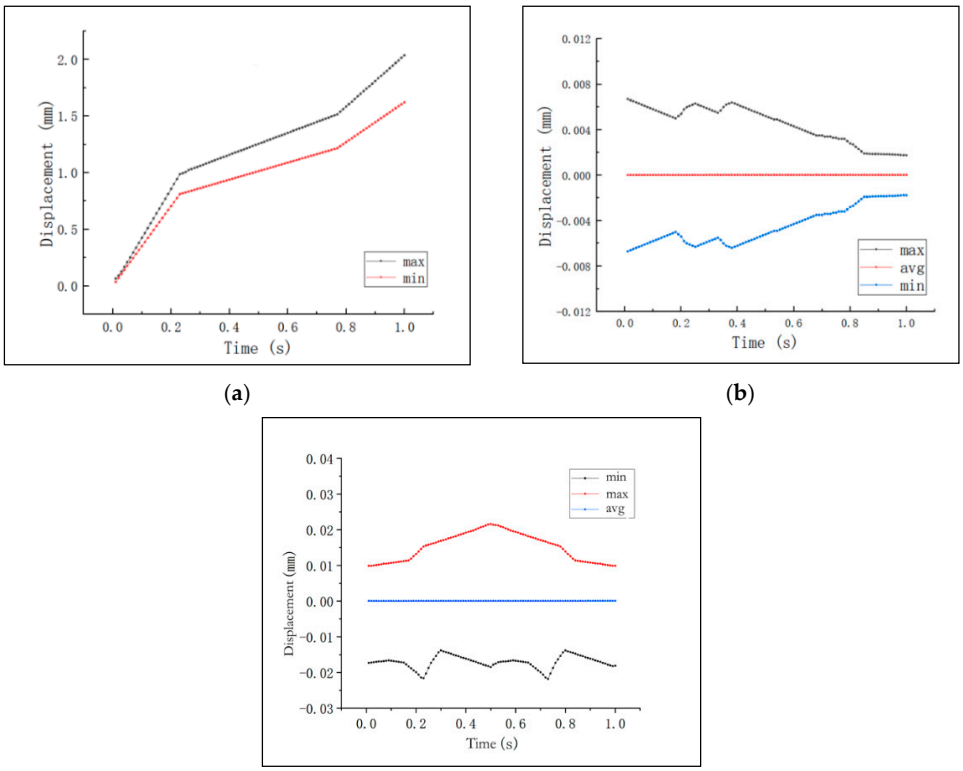

Figure 8. Motion displacement curve of *z*-axis mechanism; (**a**) the *z*-axis displacement; (**b**) the *x*-axis displacement; (**c**) the *y*-axis displacement.

(2) The nozzle head was linked with the *x*-axis and *y*-axis to analyze its motion precision and its influence on the *z*-axis when moving in the *x* and *y* directions. The nozzle moved along the *x* and *y* axes simultaneously. By moving 8 mm in the positive direction of the *x*-axis first, then moving 3 mm in the opposite direction and 10 mm in the positive direction of the *y*-axis, the final linkage effect was evaluated. The displacement curves of the *x*-axis and *y*-axis are shown in Figure 9a. The results show that the first two axes moved at the same time in 0.75 s and were relatively stable. At 0.75 s~1 s, there was an instantaneous reverse movement of *x*-axis, which had a certain influence on the interaction between the two axes. When the *x* and *y* axis was linked, the moving displacement of the nozzle in the *z*-axis direction is shown in Figure 9b. At the maximum displacement, it was still not sufficient to pose significant impact on the overall printing.

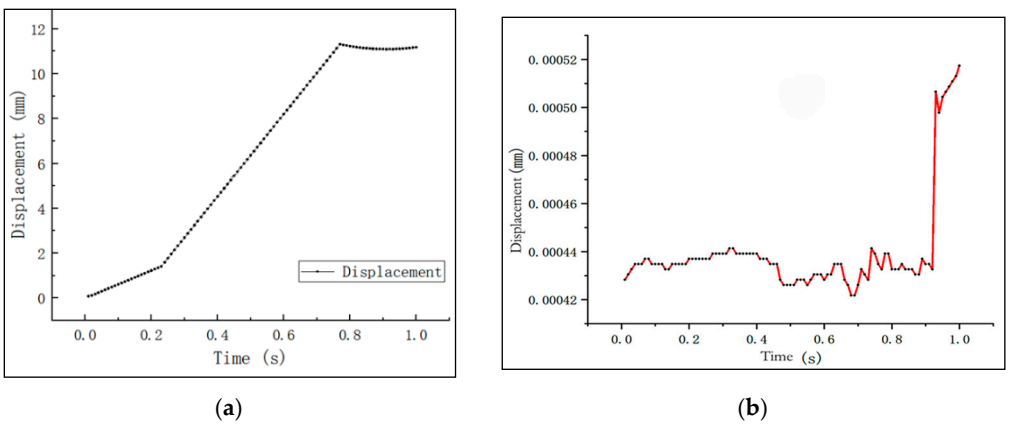

Figure 9. *x*-axis and *y*-axis linkage displacement curves. (**a**) the moving displacement of the *x* and *y* axis linked with the nozzle head; (**b**) the displacement of the *z*-axis.

(3) The printing platform drives the reversal of the platform through a parallel structure. Below the printer platform were three branches of the power sources distributed at 120°. Due to the limitation of freedom, it only rotated along the x or y axes. In transient analysis, the independent branch drive and multi-branch simultaneous drive were analyzed (Figure 10). The rotation and movement of the platform were transformed into the displacement represented at the x, y and z directions. The results showed that the printer platform ran smoothly without interference, and the moving displacement was consistent with the theoretical value.

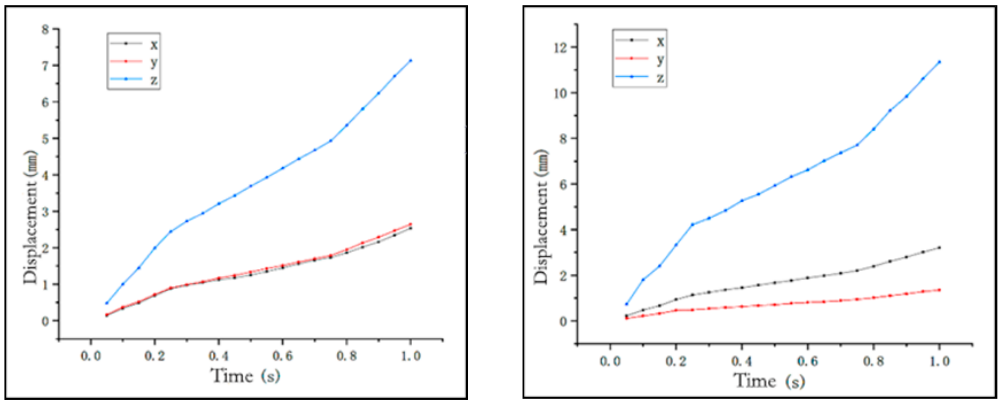

(**a**) (**b**)

Figure 10. Print platform transient analysis curve. (**a**) The moving displacement of the platform driven by a single branch; (**b**) The moving displacement of the platform driven by a multiple branches.

7. Conclusions

Based on the 3D printing of the wood fiber gel material, cellulose, hemicellulose and lignin gel materials from a branch, waste wood and wood scraps of Cunninghamia lanceolata that can be used for 3D printing were analyzed and prepared. The results showed that cellulose produced a mutation condition near 52 °C and hemicellulose produced a mutation near 80 °C. The structure of a 5-DoF hybrid three-nozzle 3D printer was designed based on the material temperature of mutation condition, and a 3D solid model was established to analyze the structural properties, mechanical properties and motion mechanics. The results showed that the 5-DoF hybrid three-nozzle 3D printing mechanism can realize the 3D printing of wood fiber gel materials. Through the analysis of the structure performance and kinematics, the correctness of the theoretical basis was verified. At the same time, the motion simulation of the structure was realized in the transient motion analysis, which confirmed the rationality of the structure.

This study is a 3D printer design and analysis for wood gel material. The wood fibers mainly contain cellulose, hemicellulose and lignin, which correspond to the three printheads of the printer, and through subsequent studies aim to achieve the solid printing of bionic wood through this type of printer. Meanwhile, the design and implementation of purely multi-jet and multi-degree-of-freedom printers can provide a reference or a direction and idea for the 3D printing industry.

Author Contributions: Formal analysis, X.S.; Investigation, J.C., G.W. and W.C.; Software, X.S.; Supervision, J.C. and G.D.; Writing—original draft, J.C. and Q.Z.; Writing—review & editing, Q.Z. All authors have read and agreed to the published version of the manuscript.

Funding: This work was supported by the National Natural Science Foundation of China (No. 51865053) and the Scientific Research Fund Project of Yunnan Provincial Education Department (No. 2022J0501).

Institutional Review Board Statement: Not applicable.

Informed Consent Statement: Not applicable.

Data Availability Statement: Not applicable.

Conflicts of Interest: The authors declare no conflict of interest.

References

1. Kalkal, A.; Kumar, S.; Kumar, P.; Pradhan, R.; Willander, M.; Packirisamy, G.; Kumar, S.; Malhotra, B.D. Recent advances in 3D printing technologies for wearable (bio)sensors. *Addit. Manuf.* **2021**, *46*, 102088. [CrossRef]
2. Lu, B.H. Additive manufacturing technology—Surrent status and future. *China Mech. Eng.* **2020**, *31*, 19–23. (In Chinese)
3. Zhao, J.Y. Development and application trends of 3D printers. *Pap. Equip. Mater.* **2020**, *49*, 114. (In Chinese)
4. Liu, Y.X.; Zhao, G.J. *Wood Science*; China Forestry Press: Beijing, China, 2012. (In Chinese)
5. Wang, Q.; Ji, C.; Sun, L.; Sun, J.; Liu, J. Cellulose Nanofibrils Filled Poly(Lactic Acid) Bio composite Filament for FDM 3D Printing. *Molecules* **2020**, *25*, 2319. [CrossRef]
6. Cao, W.T.; Ma, C.; Mao, D.S.; Zhang, J.; Ma, M.G.; Chen, F. MXene-Reinforced Cellulose Nano fibril Inks for 3D-Printed Smart Fibers and Textiles. *Adv. Funct. Mater.* **2019**, *29*, 1905898. [CrossRef]
7. Tang, A.; Liu, Y.; Wang, Q.; Chen, R.; Liu, W.; Fang, Z.; Wang, L. A new photoelectric ink based on nanocellulose/CdS quantum dots for screen-printing. *Carbohydr. Polym.* **2016**, *148*, 29–35. [CrossRef] [PubMed]
8. Gunasekera, D.H.; Kuek, S.; Hasanaj, D.; He, Y.; Tuck, C.; Croft, A.K.; Wildman, R.D. Three dimensional ink-jet printing of biomaterials using ionic liquids and co-solvents. *Faraday Discuss.* **2016**, *190*, 509–523. [CrossRef]
9. Yang, J.; An, X.; Liu, L.; Tang, S.; Cao, H.; Xu, Q.; Liu, H. Cellulose, hemicellulose, lignin, and thei r derivatives as multi-components of bio-based feedstocks for 3D printing. *Carbohydr. Polym.* **2020**, *250*, 116881. [CrossRef]
10. Xu, W.; Zhang, X.; Yang, P.; Långvik, O.; Wang, X.; Zhang, Y.; Feng, F.; Österberg, M.; Willför, S.; Xu, C. Surface Engineered Biomimetic Inks Based on UV Cross-Linkable Wood Biopolymers for 3D Printing. *ACS Appl. Mater. Interfaces* **2019**, *11*, 12389–12400.
11. Markstedt, K.; Escalante, A.; Toriz, G.; Gatenholm, P. Biomimetic Inks Based on Cellulose Nano fibrils and Cross-Linkable Xylans for 3D Printing. *ACS Appl. Mater. Interfaces* **2017**, *9*, 40878–40886. [CrossRef] [PubMed]
12. Graichen, F.H.M.; Grigsby, W.J.; Hill, S.J.; Raymond, L.G.; Sanglard, M.; Smith, D.A.; Thorlby, G.J.; Torr, K.M.; Warnes, J.M. Yes, we can make money out of lignin and other bio-based resources. *Ind. Crops Prod.* **2017**, *12*, e431. [CrossRef]
13. Ebers, L.S.; Arya, A.; Bowland, C.C.; Glasser, W.G.; Chmely, S.C.; Naskar, A.K.; Laborie, M.P. 3D printing of lignin: Challenges, opportunities and roads onward. *Biopolymers* **2021**, *112*, e23431. [CrossRef]
14. Hong, S.H.; Park, J.H.; Kim, O.Y.; Hwang, S.H. Preparation of Chemically Modified Lignin-Reinforced PLA Bio composites and Their 3D Printing Performance. *Polymers* **2021**, *13*, 667. [CrossRef]
15. Gao, X. Current status and research ideas of cellulose materials in 3D printing. *Sci. Technol. Innov. Prod.* **2020**, *7*, 56–58. (In Chinese)
16. Feng, T.; Chen, J.F.; Wang, C.; Chen, W.G. Laser-cured cellulose gel for 3D printing. *Cellul. Sci. Technol.* **2020**, *28*, 42–47. (In Chinese)
17. Kam, D.; Braner, A.; Abouzglo, A.; Larush, L.; Chiappone, A.; Shoseyov, O.; Magdassi, S. 3D Printing of Cellulose Nanocrystal-Loaded Hydrogels through Rapid Fixation by Photopolymerization. *Langmuir* **2021**, *37*, 6451–6458. [CrossRef] [PubMed]
18. Gabrielii, I.; Gatenholm, P.; Glasser, W.G.; Jain, R.K.; Kenne, L. Separation, characterization and hydrogel-formation of hemicellulose from aspen wood. *Carbohyd. Polym.* **2000**, *43*, 367–374. [CrossRef]
19. Bahçegül, E.G.; Bahçegül, E.; Özkan, N. 3D Printing of Hemicellulosic Biopolymers Extracted from Lignocellulosic Agricultural Wastes. *ACS Appl. Polym. Mater.* **2020**, *2*, 2622–2632. [CrossRef]
20. Ravishankar, K.; Venkatesan, M.; Desingh, R.P.; Mahalingam, A.; Sadhasivam, B.; Subramaniyam, R.; Dhamodharan, R. Biocompatible hydrogels of chitosan-alkali lignin for potential wound healing applications. *Mater. Sci. Eng. C Mater. Biol. Appl.* **2019**, *102*, 447–457. [CrossRef]
21. Feng, T.; Chen, J.F.; Wang, C.; Liu, B.; Chen, W.G. Design and analysis of FDM-type multi-jet 3D printers. *Digit. Print.* **2020**, *5*, 53–61. (In Chinese)
22. Lu, Y.Z.; Xu, J.F.; Chen, Y.J.; Wang, Z.G.; Ma, J.X. Effect of KH550 modification on the properties of micro-nano-cellulose/PLA composite 3D printing materials. *Chin. J. Papermak.* **2019**, *34*, 14–19. (In Chinese)
23. Zhu, J.; Zhang, Q.; Yang, T.; Liu, Y.; Liu, R. 3D printing of multi-scalable structures via high penetration near-infrared photopolymerization. *Nat. Commun.* **2020**, *11*, 3462. [CrossRef]
24. Raney, J.R.; Compton, B.G.; Mueller, J.; Ober, T.J.; Shea, K.; Lewis, J.A. Rotational 3D printing of damage-tolerant composites with programmable mechanics. *Proc. Natl. Acad. Sci. USA* **2018**, *115*, 1198–1203. [CrossRef]
25. Jiang, Y.F.; Zhao, F.Q.; Li, H.; Zhang, M.; Jiang, Z.F. Ink direct writing additive manufacturing technology and its research progress in the field of energy-containing materials. *J. Pyrotech.* **2022**, *45*, 1–19. (In Chinese)
26. Wu, C.M.; Dai, C.K.; Wang, C.L.; Liu, Y.J. Research progress of multi-degree-of-freedom 3D printing technology. *Chin. J. Comput.* **2019**, *42*, 1918–1938. (In Chinese)
27. Yu, Y.; Chen, Z.Y.; Wang, Z.M. Structure design of free switching multi-color 3D printing with three nozzles. *Modern Salt Chem. Ind.* **2021**, *48*, 185–186. (In Chinese)
28. Li, W.M.; Luo, H.B.; Zhu, H.P.; Xia, Y. Effect of moving mass velocity on the dynamic deflection response of simply supported beams. *J. Huazhong Univ. Sci. Technol. (Nat. Sci. Ed.)* **2008**, *36*, 117–120. (In Chinese)